Organic & Biomolecular Chemistry

Decomplexation as a rate-limitation in the Thiol-Michael addition of N-acrylamides

Journal:	*Organic & Biomolecular Chemistry*
Manuscript ID	OB-ART-04-2020-000726.R2
Article Type:	Paper
Date Submitted by the Author:	28-Jul-2020
Complete List of Authors:	Brown, Joseph; Massachusetts Institute of Technology, Chemistry; Cornell University, Chemical Engineering Ruttinger, Andrew; Cornell University, Chemical and Biomolecular Engineering Vaidya, Akash J; Cornell University, Chemical and Biomolecular Engineering Alabi, Christopher; Cornell University, Chemical and Biomolecular Engineering Clancy, Paulette; Johns Hopkins University, Chemical and Biomolecular Engr.

Decomplexation as a rate limitation in the thiol-Michael addition of *N*-acrylamides

Joseph S. Brown,[†,‡,a] Andrew W. Ruttinger,[‡,a] Akash J. Vaidya,[a] Christopher A. Alabi*[,a] and Paulette Clancy,*[,b]

[a] Robert F. Smith School of Chemical and Biomolecular Engineering, Cornell University, Ithaca, NY, USA, 14853

[b] Department of Chemical and Biomolecular Engineering, The Johns Hopkins University, Baltimore, MD, USA, 21218.

KEYWORDS: thiol-Michael addition, kinetics, DFT, nudged elastic band, structure-kinetic relationship, oligoTEAs

ABSTRACT: The thiol-Michael addition is a popular, selective, high-yield "click" reaction utilized for applications ranging from small-molecule synthesis to polymer or surface modification. Here, we combined experimental and quantum mechanical modeling approaches using density functional theory (DFT) to examine the thiol-Michael reaction of N-allyl-N-acrylamide monomers used to prepare sequence-defined oligothioetheramides (oligoTEAs). Experimentally, the reaction was evaluated with two fluorous tagged thiols and several monomers at room temperature (22 ºC and 40 ºC). Using the Eyring equation, the activation energies (enthalpies) were calculated, observing a wide range of energy barriers ranging from 28 kJ/mol to 108 kJ/mol within the same alkene class. Computationally, DFT coupled with the Nudged Elastic Band method was used to calculate the entire reaction coordinate of each monomer reaction using the B97-D3 functional and a hybrid implicit-explicit methanol solvation approach. The thiol-Michael reaction is traditionally rate-limited by the propagation or chain-transfer steps. However, our test case with *N*-acrylamides and fluorous thiols revealed experimental and computational data produced satisfactory agreement only when we considered a previously unconsidered step that we termed "product decomplexation," which occurs as the product physically dissociates from other co-reactants after chain transfer. Five monomers were investigated to support this finding, capturing a range of functional groups varying in alkyl chain length (methyl to hexyl) and aromaticity (benzyl and ethylenephenyl). Increased substrate alkyl chain length increased activation energy, explained by the inductive effect. Aromatic ring-stacking configurations significantly impacted the activation energy and contributed to improved molecular packing density. Hydrogen-bonding between reactants increased the activation energy emphasizing the rate-limitation of the product decomplexation. Our findings begin to describe a new structure-kinetic relationship for thiol-Michael acceptors to enable further design of reactive monomers for synthetic polymers and biomaterials.

Introduction

The thiol-ene reaction has a long history and utility in synthetic chemistry, covalently linking a thiol and an alkene to form an alkyl sulfide, often a thioether.[1–4] First applied in polymer crosslinking, the thiol-ene reaction was used most prominently in the vulcanization of rubber by the radical addition of sulfur and thiols.[2,5] Generally, this proceeds by one of two routes: i) radical addition or ii) with a base or nucleophile, known as the thiol-Michael addition.[6] The thiol-Michael addition derives from the general Michael addition,[7,8] where a carbanion or nucleophile reacts with an electron-deficient alkene in the presence of a catalyst,[7,9] and has been demonstrated in a variety of nucleophiles[9–13] and alkenes.[2–4]

As a robust "click" reaction, the thiol-Michael addition (Figure 1A) has found broad utility from materials chemistry to bioconjugation, motivating past research into the reaction mechanism.[1,6,9,14–19] Material and polymeric applications of the thiol-Michael addition include the synthesis and post-functionalization of designer polymers,[9,20,21] surface grafting,[22] nanoparticle functionalization,[23] and tissue engineering.[24]. With its tolerance to aqueous conditions, it has been utilized for bioconjugation[25] and fluorogenic probes.[26,27] The thiol-Michael addition has also been used to assemble sequence-defined oligothioetheramides (oligoTEAs).[28] OligoTEAs are prepared from *N*-allyl-*N*-acrylamide monomers via iterative reactions of the photo-initiated thiol-ene and thiol-Michael addition with dithiols on a fluorous scaffold.[28,29] The thiol-Michael addition proceeds independently of the allyl group, highlighting the differences between catalyst and alkene requirements of the two reactions.[28,29] In this scheme, the kinetic rate of the thiol-Michael addition varies, with some monomers showing quantitative conversion in 5 minutes (methyl *N*-allyl-*N*-acrylamide),[28] and other monomers requiring much longer times (*e.g.*, azido *N*-allyl-*N*-acrylamide).[30,31] Since it continues to be used to prepare complex, highly specific macromolecules including click nucleic acids (CNAs),[20] the thiol-Michael addition must remain a target of fundamental research to advance its use in precise synthetic schemes including automated,[32] flow,[33,34] and/or combinatorial split-pool syntheses.[35]

The observed rate of reaction and the rate-limiting step (RLS) of thiol-Michael addition can be substantially affected by substituent effects. In the base-catalyzed thiol-Michael addition mechanism, base concentration, pKa, sterics, solvent polarity, and pH affect reaction rate and yield.[9] In the nucleophilic mechanism, the nucleophile reacts with the Michael acceptor directly to form a strong base (*e.g.*, carbanion) through an initiation step to generate thiolate.[9] Generally, the rates for nucleophile-initiated reactions are faster than with base-catalysis, commonly achieved with unhindered amines and phosphines (*e.g.,* dimethylphenyl phosphine (DMPP)

used in this study) both in experimental and theoretical comparisons.[9,17,36–43] The overall reaction rate increases as the catalyst participates more in the nucleophile-initiated mechanism.[41,44] For the thiol-Michael addition, steric hinderance or lack of electron-deficiency of the alkene can generally slow the reaction.[15] Generally, polar aprotic solvents are preferred for the thiol-Michael addition reaction to stabilize charged intermediates without interfering with proton transfer steps for either catalyzed reaction.[45]

However, there are variations in the reported RLS. The thiolate attack (propagation) has been commonly considered the RLS,[9,15] while other reports have argued the proton transfer to the carbanion (chain transfer),[44] or the nucleophile attack on the alkene (initiation) can be slower.[36] There is also lack of agreement on reversibility of the reaction. Most reports agree that the thiolate attack is reversible;[9,15] some researchers suggest the entire Michael addition is reversible.[43,46,47] Additionally, recent work by M-F Reyniers *et al.* has suggested diffusion limitations, as opposed to reactive limitation found for liquid-phase thiol-Michael reactions.[13,44]

To better understand the variability of this reaction, we performed a combined experimental and computational mechanistic study to reveal structural contributions across a variety of monomers that led to wide-ranging differences in reaction kinetics. After a review of the current understanding of the thiol-Michael addition kinetics and mechanism, we analyzed the thiol-Michael addition mechanism of a fluorous hydroxylated thiol with a butyl *N*-allyl-*N*-acrylamide monomer used in the assembly of oligoTEAs. We found that the RLS for this reaction was the decomplexation of the thioether product from the co-reactants after chain transfer, a step previously unconsidered in literature but necessary for this cyclic reaction. To further test the validity of this product decomplexation as the RLS, we extended this analysis to other monomers with different functional groups, demonstrating consistent support and structural influences on the kinetic finding. Further examination of the structural contributions to the configurations of the transition state revealed the importance of hydrogen bonding and conformation (e.g., aromatic stacking) as a key modulator. Overall, the rate-limitation of the product decomplexation was emphasized with hydrogen-bonding from the hydroxylated thiol, and more comparable to the traditional rate limiting step of propagation with a standard alkyl thiol.

Results and Discussion

We have focused on investigating the mechanism of the nucleophile-initiated thiol-Michael addition utilizing a phosphine catalyst, DMPP, which does not undergo the base-catalyzed mechanism. We considered the following steps: i) the nucleophile attacks the electron *N*-deficient alkene, resulting in a carbanion, ii) the carbanion extracts a proton from a thiol to generate a thiolate (initiation), iii) the thiolate attacks another electron *N*-deficient alkene, forming another carbanion (propagation), iv) the new carbanion is stabilized through a second proton transfer from an additional thiol, generating a new thiolate and the desired product (chain transfer) (Figure 1B). Overall, the thiol-Michael addition proceeds at a constant concentration of anionic species within the common mechanism, similar to other living polymerizations. Since this scheme is widely considered to apply, our research focused on determining substituent effects that direct the RLS.[9,36,42,44]

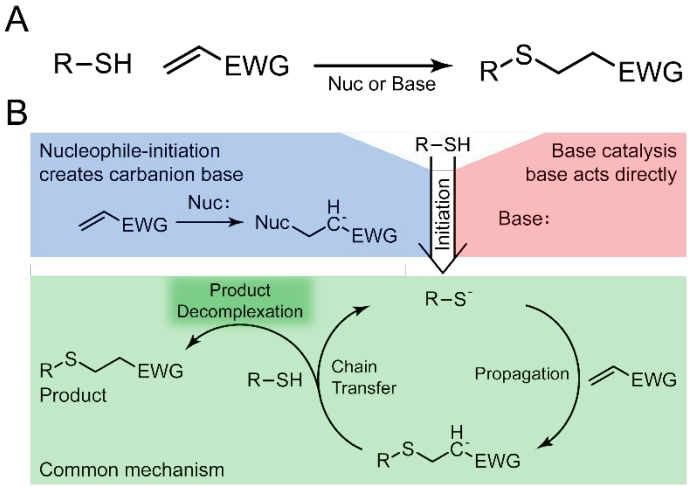

Figure 1. A. The generalized thiol-Michael addition. EWG: electron withdrawing group; Nuc: Nucleophile. **B.** Nucleophile initiation is shown in blue (typical for dimethylphenyl phosphine DMPP used in this study), base initiation in red, and the cyclic common mechanism in light green. The green highlight specifically labels the product decomplexation step.

Experiments were completed to measure the thiol-Michael addition reaction using methyl, butyl, hexyl, benzyl, and ethylenephenyl *N*-allyl-*N*-acrylamides, based on their ability to show an increasing alkyl substituent effect[48,49] and aromaticity,[50,51] which was qualitatively known to affect reaction rate. Though not a common solvent for the thiol-Michael addition, methanol was used for all of this work as it is the primary solvent for oligoTEA assembly to solubilize all monomers and catalysts, enable direct transfer to fluorous solid-phase extraction (FSPE) purification, and provide rapid evaporation. Dimethylphenylphosphine (DMPP) was incubated with the *N*-allyl-*N*-acrylamide for quantitative carbanion formation (see Methods and Supplemental Information), allowing observation of the rate of the initiation and common mechanism (Figure 1B). The kinetic rate of the *N*-allyl-*N*-acrylamides varied significantly (Figure 2A). The methyl monomer reacted significantly faster than the other alkyl monomers, with a decreasing reaction rate observed for longer alkyl chains. But the effect did not persist significantly, as the butyl and hexyl functional groups

demonstrated statistically similar reaction speeds at both temperatures (see Supplemental Information, Table S5). The methyl and ethylenephenyl monomers had similar reaction rates at both temperatures ($p = 0.11$ and $p = 0.20$ for T = 25 and 40°C, respectively). However, there were large significant differences between the ethylenephenyl and the benzyl monomer, which rapidly increased in reaction rate with the addition of heat ($p = 0.004$ and $p = 0.026$ for T = 25 and 40°C, respectively). Usually, studies that investigate the kinetics of the thiol-Michael addition report on differences across alkene classes (*e.g.,* vinyl sulfone vs. acrylates)[38,42,52] or different catalysts (*e.g.,* amines vs. phosphines).[27,36,43,53] To the best of our knowledge, such large kinetic rate differences have not been observed within the same alkene class.

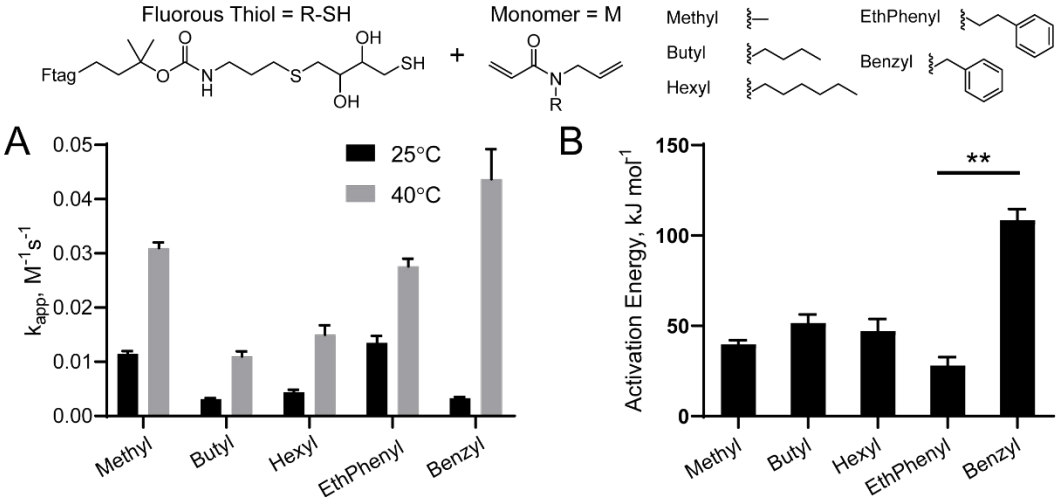

Figure 2. A. Experimental apparent kinetic rates for all monomers in the reaction outlined at 25°C and 40°C observed at a 30 mM reaction in MeOH with 1 equivalents (eqv) of fluorous thiol (F-DTT), 2 eqv of *N*-allyl-*N*-acrylamide, and 0.1 eqv of dimethylphenylphosphine (DMPP, 5 mol% relative to the *N*-allyl-*N*-acrylamide). Methanol was used to enable solubility of all monomers and catalysts, direct transfer to fluorous purification, and evaporation used in oligothioetheramide (oligoTEA) assembly. DMPP and *N*-allyl-*N*-acrylamide and were incubated for 15 minutes prior to the addition of fluorous thiol and reaction time start to ensure all reactions started at a constant carbanion concentration. Independent replicates were *n=6,3,3,3,2* and *n=4,3,3,2,3* for the methyl, butyl, hexyl, ethylenephenyl, and benzyl at RT and 40ºC, respectively (see Methods and Supplemental Information, Table S5 for statistical summary). **B.** The corresponding apparent activation energies (enthalpies) calculated through the Eyring equation with the Gibbs free energy substitution with ethylenephenyl and Benzyl demonstrating a large significant difference (** indicates $p < 0.01$, $p = 0.0066$, $df = 1.84$, $n = 2$).

To better understand these effects and the underlying mechanism, we employed Density Functional Theory (DFT) in conjunction with Nudged Elastic Band (NEB) methods to determine reaction energies and energy barriers, similar to other studies that looked at alkene class or catalyst effects.[36,44,48,54] We use a hybrid implicit-explicit solvation model with four explicit molecules to account for the effect of methanol on the studied reaction mechanisms. Prior to our study, we verified the choice of DFT functional through benchmarking with a study based on functional performance in thiol-Michael addition systems.[54–56] Here, we compared the B97-D3 functional with ωB97X-D3, which has been shown to be accurate for thiol systems, and showed excellent agreement for prediction of both the C-S bond length and the energy of the carbanion intermediate, prior to the propagation step. (Figure S2) This expected behavior of our selected B97-D3 functional allowed us to confidently move forward with our mechanistic study. Experimental activation energies (enthalpies) were calculated via the Eyring equation with the Gibbs free energy substitution (Figure 2B, see Supporting Information). The comparison of the energy of our computationally derived RLS provided validation for this mechanistic study.

We took care to ensure that the computed structures were not only minimized to their minimum energy structure but that alternative reaction pathways were considered. Given sufficient sampling, the lowest energy reactant structure could be chosen confidently to find the minimum energy structure for subsequent steps in the mechanism. The existence of hydrogen-bonding between molecules was determined to be an important factor in complexation energy. Therefore, different conformations based on hydrogen-bonding networks were identified as the most plausible structures. In total, four major conformations of varying O-H-N and O-H-O bonds proved most stable, with our final conformation featuring two O-H-O hydrogen-bonds as the lowest energy structure. Other conformations without hydrogen-bonding were also considered, but were found to be less favorable. The calculated ground-state energies also demonstrated that minimizing the distance between the cationic and anionic groups was favored. We then evaluated the direct substitution of the thiolate onto the phosphine-monomer carbanion to form the desired product also considered by Frayne *et al*.[17] However, this path experienced an energy barrier larger than 200 kJ/mol (methyl *N*-allyl-*N*-acrylamide, Figure S4), significantly above our experimentally determined energies. Moreover, this reaction would consume thiolate, suggesting it to be a possible termination reaction. Thus, the traditional mechanism presented in literature, outlined in Figure 1, appeared most likely to fit our observations of thiol-Michael addition.

Next, we performed a full mechanistic study for a model butyl *N*-allyl-*N*-acrylamide monomer to measure agreement between experiment and simulation (Figure 3). We found poor agreement with the experimental data (Figure 4). Our results showed the propagation step could be rate-limiting, matching reports from Nair *et al*. and Mather *et al*.[9,15] However, the size of the propagation barrier (29.7 kJ/mol) was still significantly different from our experimental value (51.6 ± 4.8 kJ/mol). Thus, we analyzed the reaction behavior at a molecular-scale, following the anionic charge transfer and noting several molecular complexations along the pathway.

Our reaction coordinate started with the zwitterionic phosphine initiator (I±), prepared from the phosphine initiator (I) reacted with the butyl *N*-allyl-*N*-acrylamide to the point of completion (5 mol%), as a source of carbanion base (Figure 1 in blue). Here, the carbanion of the zwitterionic phosphine initiator acts as a Brønsted-Lowry base, extracting a proton from the thiol (T), making thiolate and spent phosphine initiator (I+) as the 'Initiation Proton Transfer' in Figure 3 and 4. The anionic charge located on the thiolate (T-), electrostatically stabilized its complexation with the cationic spent phosphine initiator (I+).

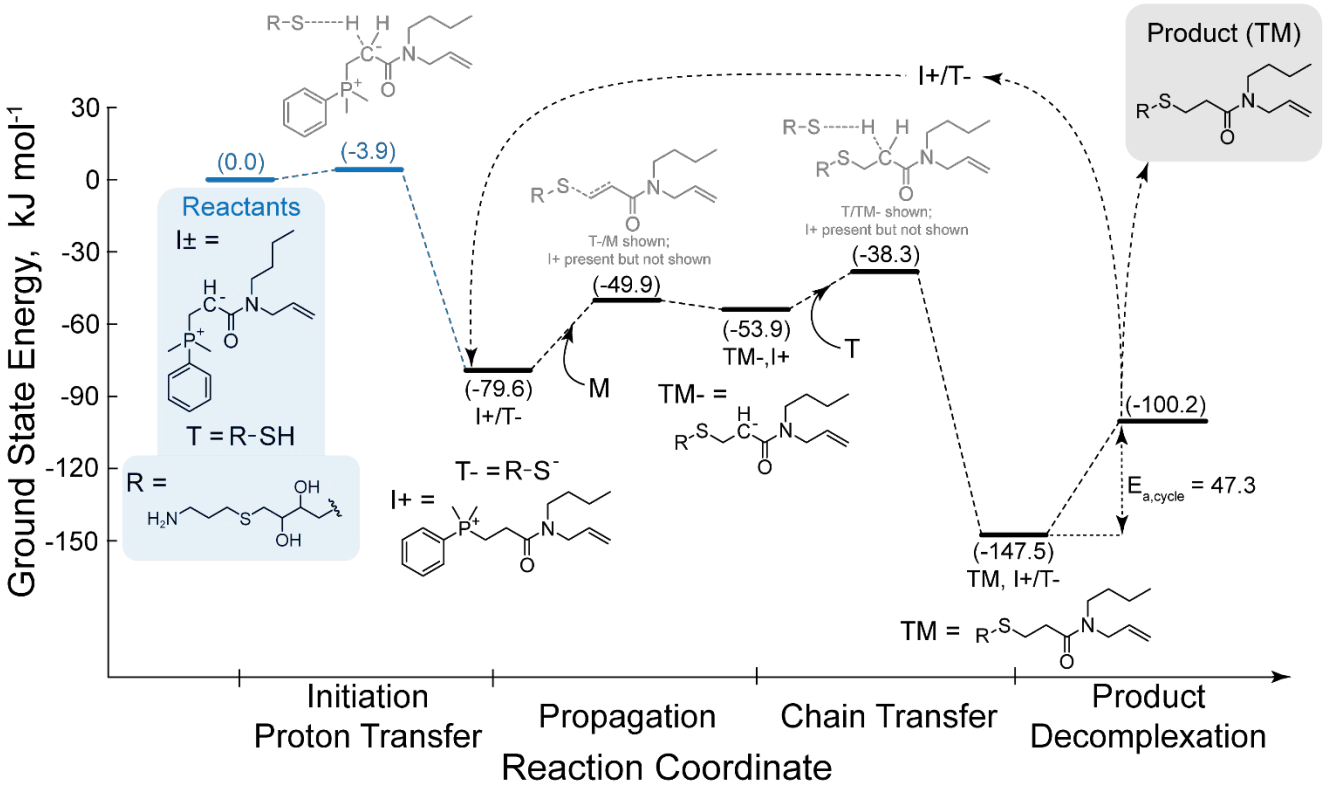

Figure 3. The energy profile of the reaction mechanism of butyl *N*-allyl-*N*-acrylamide monomer undergoing a thiol-Michael addition with the fluorous thiol. All reaction energies were calculated using DFT with a hybrid implicit-explicit solvation model with four explicit molecules (See Methods and Supporting Information). The initiation step is provided in blue with the initiation proton transfer calculated separately from the nucleophile attack onto the *N*-acrylamide similar to the experimental starting point. Cyclic steps are shown in black. At the end of the product decomplexation step, a fresh alkene monomer (M) would replace the newly formed product (TM) and return the cycle to the propagation step. Atomic configurations are provided, with transition state complexes shown in gray above the reaction coordinate line and reaction intermediates below.

Next, propagation and chain transfer were considered. During propagation, the thiolate (T-) attacked the alkene of an unreacted butyl *N*-allyl-*N*-acrylamide (M) to generate a carbanion (TM-) intermediate. The energy required to separate the thiolate-phosphonium complex (T/I+) was much higher than that for the neutral butyl *N*-allyl-*N*-acrylamide (M) to approach the electrostatically stabilized complex. Experimentally, the monomer was also present in two-fold excess, which further supported this proposed pathway. Thus, the unreacted butyl *N*-allyl-*N*-acrylamide approached and thiolate attack proceeded, propagating the anion charge onto the carbanionic product (TM-). The carbanionic product (TM-) is stabilized by the spent phosphine initator (I+) in this complex and, thus, it was more favorable for another thiol (T) to approach for the chain transfer to occur. With the addition of new thiol (T), the carbanionic product (TM-) extracted the proton from the thiol (T), making product (TM) and a new thiolate (T-), in a chain transfer step of the anion.

In order to continue the thiol-Michael addition cycle, the product (TM) must be removed from its electrostatically stabilized complex, also containing the spent phosphine initiator (I+) and new thiolate (T-), to allow a new alkene monomer to react. This step can be referred to as the "product decomplexation" and the energy barrier associated with this molecular dissociation was calculated. By considering the product decomplexation barrier (47.3 kJ/mol), our computational results now showed good agreement with experiment (51.6 ± 4.8 kJ/mol), being within the experimental error. The slight underprediction in energy by the computations is likely due to the approximation of the product decomplexation energy barrier as the energy difference between a complexed and fully decomplexed product, which may overlook a small barrier along the energy pathway. Moreover, the energy barrier of product

decomplexation was sufficiently larger than the propagation energy barrier, allowing us to confidently label "product decomplexation" as an important contributor to the observed reaction rate. Upon completion of this cycle, a fresh alkene monomer would bind to the thiolate-phosphonium complex, returning the mechanism to the intermediate prior to propagation and beginning the next cycle.

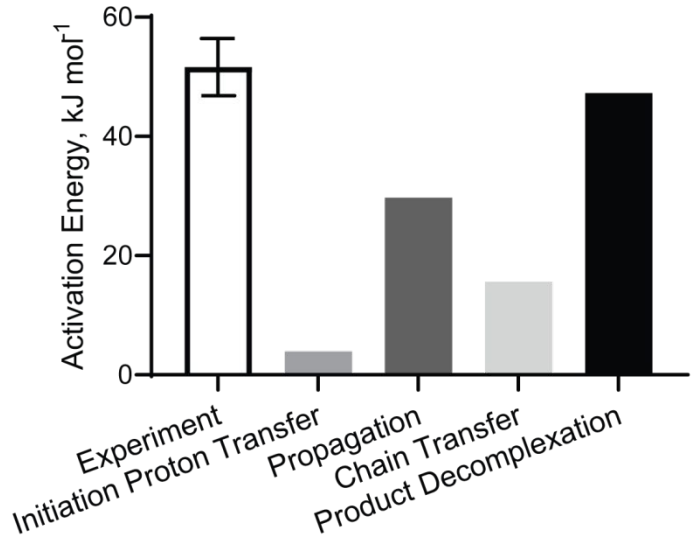

Figure 4. Comparison of all energy barriers for the reaction of the fluorous thiol and butyl *N*-allyl-*N*-acrylamide calculated using DFT corresponding to the atomistic configurations shown in Figure 3 with an explicit methanol solvent (see Methods and Supporting Information) against experimental values.

Thus, we extended our mechanistic study to look at additional functional groups for further validation: methyl, hexyl, benzyl, and ethylenephenyl, capturing effects of both chain length and aromaticity on *N*-allyl-*N*-acrylamides. For all functional groups (Figure 5A), the heats of reaction for initiation proton transfer and chain transfer are highly exothermic, expected for a stable proton transfer. However, the propagation is endothermic with a relatively small energy barrier in the reverse direction. Thus, the entire thiol-Michael addition is unlikely to be reversible, though the propagation step could be reversible, echoing the kinetic importance of the propagation step.[9,15]

In line with our studies for the butyl *N*-allyl-*N*-acrylamide monomer, results for the additional functional groups exhibited a product decomplexation RLS (Figure 5). For the alkyl chains, good agreement was observed between computation and the experimental mean ranges, differing by 1-5 kJ/mol. The overprediction of ethylenephenyl is more significant (18 kJ/mol), as is the underprediction of benzyl (48 kJ/mol). However, previous studies have highlighted the difficulty for certain functionals to properly describe aromatic stacking energies.[57] The computationally predicted propagation barrier for the ethylenephenyl group also exceeds the experimental value by 7 kJ/mol. While the likely explanation is that our calculations miss the MEP, the product decomplexation barrier still dominates as the largest energy barrier, in line with the other functional groups as a main contributor to the observed reaction rate. Previous work has also outlined the challenge of obtaining quantitatively accurate computational energies in complex multimolecular polar reactions in an alcohol solvent.[58] However, those authors also acknowledged that these challenges are not necessarily greater than those seen in other computational studies in solvents. At the very least, given the quantitative agreement with experiment, our results suggest that these computational results provide a meaningful representation of reaction energies. Furthermore, our reaction energies provide strong evidence regarding trends across the functional groups we studied.

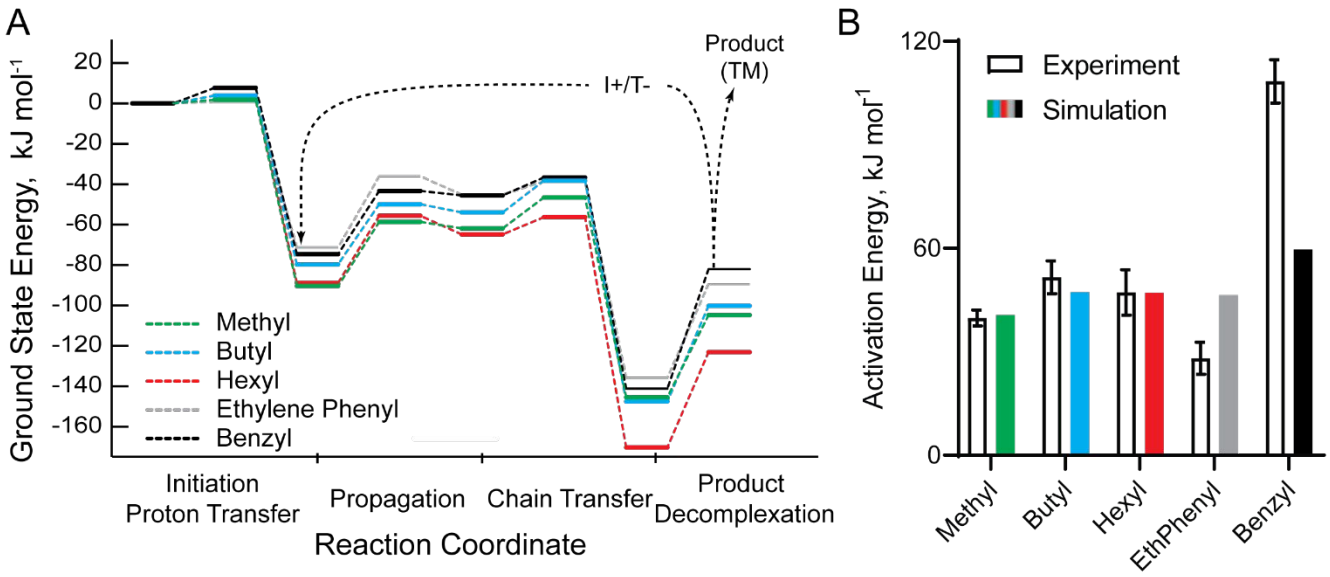

Figure 5. A. The energy profile of the reaction mechanism for our five studied monomers undergoing a thiol-Michael addition: methyl, butyl, hexyl, ethylenephenyl, and benzyl. A legend is provided in the bottom left corner. All reaction energies were calculated using DFT. A black dashed line is provided to signify the cyclic nature of the latter three steps for each mechanism. **B.** The rate-limiting reaction energies for each studied mechanism (product decomplexation). Experimental bar chart values are shown with no fill. Simulation bar chart values are shown with color fills corresponding to their color in A. Error bars represent experimental error propagated *n=4,3,3,2,2* for the methyl, butyl, hexyl, ethylenephenyl, and benzyl, respectively.

We observed trends within the particular families of functional groups (Figure 5B). The energy barrier increased as the length of the alkyl chain increased toward an asymptotic value. One possible explanation is the inductive effect, the electronic effect of atomic groups due to bond polarization, also observed in literature.[49,59,60] A recent study found the inductive effect to be saturated at an alkyl chain length of four or more (butyl),[61] consistent with our results. A noticeable (7 kJ/mol) gap was observed between the reaction energies for methyl and butyl variants, but no gap (0 kJ/mol) between butyl and hexyl. The effect of aromaticity was highlighted by comparing hexyl and benzyl groups, which both contain six carbons. The reaction energy for hexyl was 47 kJ/mol, whereas the aromatic benzyl more than doubled the reaction energy to 108 kJ/mol. This result is likely due to attractive aromatic stacking between the DMPP and *N*-allyl-*N*-acrylamide monomer that stabilizes reaction intermediates,[62] as well as increased steric hindrance, leading to higher reaction energies. However, these results do not clarify the difference between benzyl (108 kJ/mol) and ethylenephenyl (28 kJ/mol), despite the effect of aromatic stacking/interactions.

A closer look at the benzyl and ethylenephenyl aromatic stacking provides insight into their different observed reaction energies. Literature describes four configurations for aromatic stacking, characterized by their separation and the angle formed between their flat planes.[50] Out of the four configurations, the "parallel-displaced" and "T-stacking" are invariably the most stable, with predicted interaction energies of ~11.5 kJ/mol.[62] Our calculations predicted a T-stacking configuration for the ethylenephenyl *N*-allyl-*N*-acrylamide mechanism (Figure 6A,6C, Tables S1,S2). [51,62] In contrast, the benzyl *N*-allyl-*N*-acrylamide preferred to adopt a parallel-displaced configuration, with closer packing (Figure 6B,6C, Tables S1,S2). The additional carbon group on the ethylenephenyl group provided more separation between benzene rings, affecting the stacking configuration. While the isolated interaction energy of T-stacking and parallel displaced is indistinguishable,[62] the parallel-displaced configuration for the benzyl *N*-allyl-*N*-acrylamide gives rise to stronger intermolecular interactions, such as hydrogen bonding, due to its closer proximity. Furthermore, after the chain transfer step of the ethylenephenyl mechanism, stacking is sterically frustrated, while stacking in the benzyl mechanism still persists. This lack of aromatic interaction in the complex prior to the product decomplexation step in the ethylenephenyl mechanism agrees with our observation of a lower energy barrier. Thus, differences in stacking configuration can be significant in terms of driving differences between the benzyl and ethylenephenyl reaction energy.

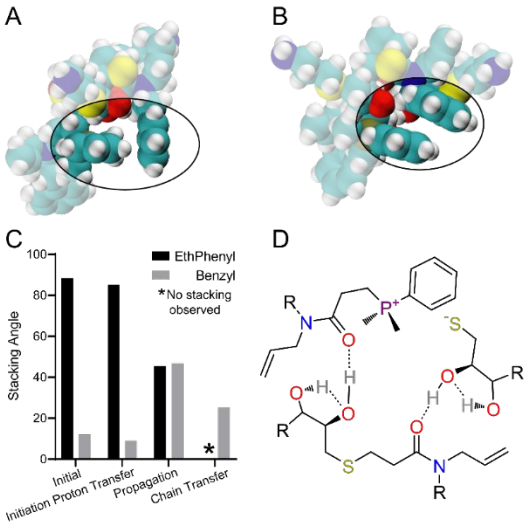

Figure 6. Aromatic stacking between molecules in a thiol-Michael addition. **A.** T-stacking configuration for ethylenephenyl *N*-allyl-*N*-acrylamide. **B.** Parallel-displaced configuration for benzyl *N*-allyl-*N*-acrylamide (right). These representations correspond to the initial configurations. **C.** The angle between stacking benzene rings are compared for the benzyl and ethylenephenyl groups as the structures evolve through the reaction. The category labels refer to the stable intermediate formed after the listed step. (See Tables S1-S2 for exact numbers) **D.** Hydrogen bonding in the thiol-Michael addition to our *N*-allyl-*N*-acrylamide monomers. The hydrogen bonds are shown by dashed black lines. These hydrogen bonds stabilize the reactive complex and result in larger energy barriers.

The effect of hydrogen bonding was found to be a significant contributor to the reaction energy. Studies have shown hydrogen bonds to have energies ranging from 4.2-42 kJ/mol,[63] with an average energy of 20.9 kJ/mol.[64] Hydrogen bond complexation can also significantly stabilize molecules in a complex, in one published case as much as 133 kJ/mol.[65] Our calculations reflect these observations, predicting hydrogen bonding between the nucleophile and hydroxyl group on the product, as well as between the carbonyl group on the product and the thiolate molecule (Figure 6D). Complexation preceded any reaction due to its significantly favorable binding energy (139 kJ/mol for the methyl reaction). Once complexed, these intramolecular hydrogen bonds were affected by proton transfers to the nucleophile and alkene monomer. However, hydrogen bonding persisted throughout the entirety of the chemical rearrangement until they were required to be severed during the product decomplexation step. Since the energy of complexation is favorable, the decomplexation energy is high, explaining product decomplexation as a main contributor to the reaction rate. Two exceptions to this observation occur after the chain transfer step in the methyl and ethylenephenyl mechanism, both with lower activation energies overall. Rather than form a hydrogen-bonded complex with catalyst, newly formed thiolate, and product, the complex for the methyl and ethylenephenyl were more stable without the hydrogen bond donated by the thiolate. We validated this observation through hydrogen *N*-acceptor bond length, with the bond lengths in methyl and ethylenephenyl increasing from 1.69 Å to 2.23 Å and from 1.63 Å to 2.35 Å, respectively. This observation provides a well-founded reasoning for the lower reaction energies of the methyl and ethylenephenyl mechanisms.

With hydrogen bonding increasing the decomplexation energy barrier, its role in reaction energy was a major consideration in our mechanism. However, alkyl-alkyl interactions, alkyl-aromatic interactions, and sulfur-based interactions[66] would still be present to maintain favorable complexation. To explore this, we analyzed the methyl *N*-allyl-*N*-acrylamide thiol-Michael reaction with a fluorous alkyl thiol, rather than our previously used fluorous hydroxylated thiol (Figure 7). From a mechanistic standpoint, this also allowed us to conclude whether the product decomplexation was a result of strong intermolecular interactions, or if it can be considered as the rule, rather than the exception.

Without hydrogen bonding in the complex, the energy barrier for the product decomplexation as the rate-limiting step dropped significantly, as well as other steps. When compared with the experimental energy barrier (17.8 kJ/mol), the product decomplexation is overpredicted by theory (29.2 kJ/mol). By isolating this hydrogen-bonding effect, we can conclude that hydrogen bonds slow the kinetics by increasing the final activation energy, in our case by 12 kJ/mol, similar to literature values.[64,65] The computed activation energy of the propagation is much closer to the product decomplexation with the alkyl thiol. This finding highlights that the propagation could be limiting for other substrates with less potential for intermolecular complexation, consistent with the traditional view in literature. Larger substrates, such as those used in the present study, could increase the dominance of the rate-limitation caused by product decomplexation.

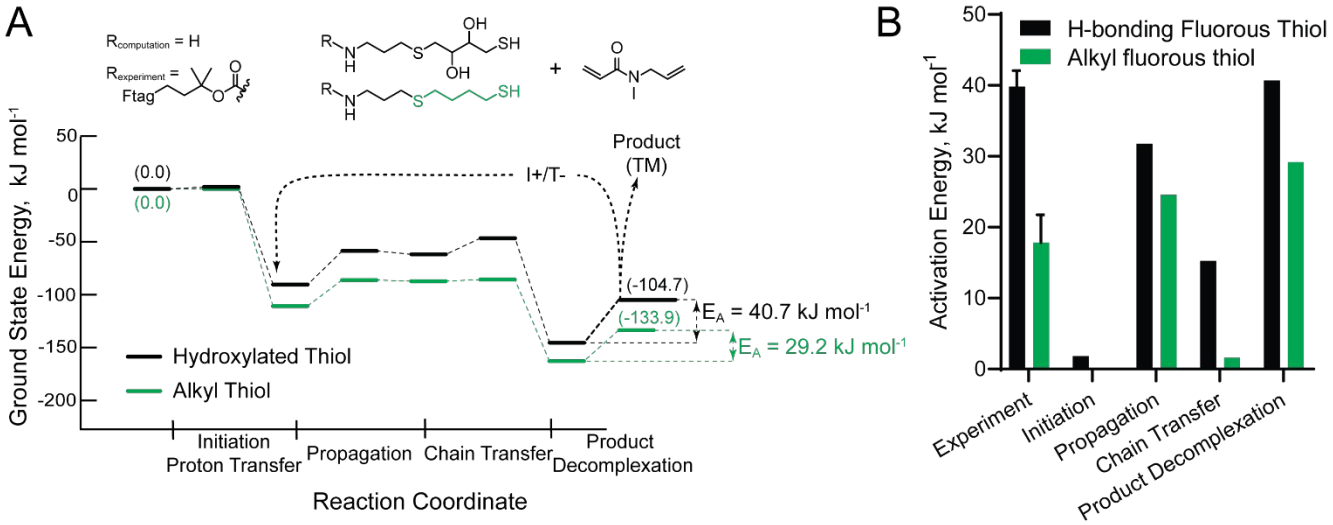

Figure 7. A. The energy profile of the reaction mechanism for the thiol-Michael addition with (black) and without (green) hydrogen-bonds. All reaction energies were calculated using DFT with an explicit methanol solvent. **B.** The reaction energies for each step in both mechanisms, along with the experimental energy barriers Replicates are *n=4,2* for the activation energy calculated for the methyl monomer reacted with the H-bonding fluorous thiol (F-DTT) and the alkyl fluorous thiol (F-BDT), respectively.

Conclusions

Precise understanding of chemical reaction kinetics can unlock advanced synthesis schemes for automated, flow, and/or combinatorial chemistry. In this spirit, we have explored an integrated experimental and computational study to investigate the mechanism for the thiol-Michael addition, providing atomic-scale insight into its underlying kinetics. Good agreement between computational and experimental activation energies was achieved only when we considered an additional, previously unstudied, structural transition that we term "product decomplexation." All *N*-allyl-*N*-acrylamide monomers reacted with a hydroxylated thiol demonstrated a product decomplexation that strongly influences the reaction rate in each case, and effectively reproduced experimentally observed functional group trends with reasonable quantitative accuracy. Calculations of the reaction with an alkyl thiol still indicated the product decomplexation as the dominant energetic barrier, but showed how the traditional RLS of propagation could also be seen as a potential rate-limiting step.

The DFT-derived data deconstructed the overall thiol-Michael mechanism into a set of chemical and physical transformations, some resolved at the atomic level. Chemically, aliphatic chain length provided an inductive effect, increasing the activation energy until it reached an asymptotic value after a length of four carbon atoms. Structurally, aromatic monomers demonstrated a larger separation between stacked benzene rings (ethylenephenyl vs. benzyl), leading to a T-stacking vs. parallel-displaced configuration, respectively. The consequence is a high energy barrier for the benzyl reaction relative to the ethylenephenyl. Our observations suggest that monomer structure can be tuned to generate important macroscopic effects such as faster kinetics, as we have measured, and a lower density of molecular packing.[67] Aromatic groups connected to the monomer backbone by longer aliphatic chains reduce the proximity of the complex stacking effects we observed. If the aliphatic chains were lengthened, we predict the kinetics to be quantitatively similar to those observed with alkyl chain groups. Additionally, hydrogen-bonding led to a high energy barrier associated with product decomplexation due to the need to break hydrogen-bonds. Through comparison between a hydroxylated thiol and an alkyl thiol for the methyl *N*-allyl-*N*-acrylamide mechanism, we show that hydrogen *N*-bonding can lead to a significant increase reaction energy by 12 kJ/mol.

Overall, our work highlights new variables that researchers can use to prepare highly reactive and selective monomers for the thiol-Michael addition, employing geometric and electronic contributions, beyond consideration of their chemical contributions. Specifically, we predict that thiol-Michael addition reactants that favor complexation, such as those containing hydroxyl groups, aromatic groups, or large inductive groups will slow down reaction kinetics. Conversely, disruption of this complexation can speed up kinetics, such as the steric effect of T-stacking for the ethylenephenyl *N*-allyl-*N*-acrylamide group, or removal of non-covalent interactions. Our efforts were focused to validate these observations rigorously, but additional future work should explore if the decomplexation is generalizable with other solvents, initiators, thiols, and Michael-acceptors. In addition, future models should consider solvation models that can explicity and fully solvate the reactive species, allowing for more accurate representations of the solvent medium. Our results will allow researchers using the thiol-Michael addition for synthesis to tune a desirable product outcome by optimizing the kinetics via these chemical effects.

Methods

Experimental. General chemicals were purchased from Sigma Aldrich, Alfa Aesar, or Acros Organics. Fluorous tag and fluorous silica were purchased from Boron Specialties. Routine NMR spectra were recorded on INOVA 400, 500, or 600 MHz spectrometers and analyzed by MestReNova (version 12.0.3). ^{1}H NMR chemical shifts are reported in units of ppm relative to the

deuterated solvent. LCMS experiments were carried out on an Agilent 1100 LCMS system with a Poreshell 120 EC-C18 (3.0x100mm, 2.7um) column monitoring at 210nm with positive mode for detection. Solvents for LCMS were water with 0.1% acetic acid (solvent A) and acetonitrile with 0.1% acetic acid (solvent B). A flow rate of 0.6 mL/min was used with a gradient starting at 5% solvent B, followed by a linear gradient of 5% to 95% solvent B over 10 min, 95% solvent B for 2 min, before returning to 0% solvent B over 2 min. Tabulated data and statistics were processed with GraphPad Prism 7.05. At points were *n=2* and *n=3* data were compared, *n=2* was assumed as the minimum possible comparison.

Preparation of N-allyl-N-acrylamides. All monomers were synthesized, purified, and confirmed as previously described, with minor modifications.[28] Methyl *N*-allyl-*N*-acrylamide was produced without modification of literature protocol through the acylation of N-allylmethylamine. Butyl, ethylenephenyl, and benzyl *N*-allyl-*N*-acrylamides were produced with the modification of acylation and then alkylation presented in literature.[68] Monomers were purified by flash chromatography using a gradient of 0-70% ethyl acetate in hexanes. Monomer fractions were collected and dried under vacuum (5 mbar) in a room temperature water bath (25C) to minimize any potential degradation. Monomers were used within 1 week of purification and stored at -20°C. Raw NMR and LCMS spectra are provided in the supporting information.

Methyl *N*-allyl-*N*-acrylamide. Viscous pale-yellow oil. ^{1}H NMR (600 MHz, Chloroform-d) δ 6.51 (m, 1H), 6.29 (m, 1H), 5.73 (m, 1H), 5.63 (m, 1H), 5.15 (m, 2H), 3.98 (m, 2H), 2.97 (d, J = 17.6 Hz, 3H). LCMS, calculated for $(M+H)^+$ 126.09, observed 125.05.

Butyl *N*-allyl-*N*-acrylamide. Viscous pale-yellow oil. ^{1}H NMR (600 MHz, Chloroform-*d*) δ 6.52 (d, 1H), 6.35 (m, 1H), 5.79 (m, 1H), 5.67 (ddd, J_1 = 28.1 Hz, J_2 = 10.6 Hz, J_3 = 2.0 Hz, 1H), 5.18 (m, 2H), 4.00 (m, 2H), 3.34 (m, 2H), 1.54 (m, 2H), 1.32 (m, 2H), 0.94 (dd, $J_{1,2}$ = 7.21). LCMS, calculated for $(M+H)^+$ 168.14, observed 168.1.

Hexyl *N*-allyl-*N*-acrylamide. Viscous pale-yellow oil. ^{1}H NMR (600 MHz, Chloroform-*d*) δ 6.52 (m, 1H), 6.35 (m, 1H), 5.80 (m, 1H), 5.67 (ddd, J_1 = 28.7 Hz, J_2 = 10.4 Hz, J_3 = 2.0 Hz, 1H), 5.18 (m, 2H), 4.00 (m, 2H), 3.33 (m, 2H), 1.55 (m, 2H), 1.29 (m, 6H), 0.88 (m, 3H). LCMS, calculated for $(M+H)^+$ 196.17, observed 196.2.

Ethylene phenyl *N*-allyl-*N*-acrylamide. Viscous yellow oil. ^{1}H NMR (600 MHz, Chloroform-*d*) δ 7.38 – 7.10 (m, 5H), 6.46 (m, 1H), 6.34 (m, 1H), 5.78 (m, 1H), 5.66 (m, 1H), 5.14 (m, 2H), 3.92 (m, 2H), 3.58 (m, 2H), 2.88 (m, 2H). LCMS, calculated for $(M+H)^+$ 216.14; observed 216.2.

Benzyl *N*-allyl-*N*-acrylamide. Viscous yellow oil. ^{1}H NMR (600 MHz, Chloroform-*d*) δ 7.48 – 7.11 (m, 5H), 6.49 (m, 2H), 5.77 (m, 2H), 5.19 (s, 2H), 4.62 (d, J = 46.5 Hz, 2H), 3.98 (m, 2H). LCMS, calculated for $(M+H)^+$ 202.12; observed 202.2.

Preparation of fluorous thiol. 2-[2-(1H,1H,2H,2H-Perfluoro-9-methyldecyl)isopropoxycarbonyloxyimino]-2-phenylacetonitrile (fluorous tag) was dissolved in THF (10 mg/mL). Two equivalents of allyl amine and two equivalents of triethylamine were added to the reaction mixture and stirred at room temperature for at least 3 hours. Afterward, the THF was completely removed by vacuum centrifuge (SpeedVac) and the reaction mixture was dissolved in fluorophobic 20% Water in MeOH wash solution, directly loaded onto fluorous silica, and purified by fluorous solid-phase extraction (FSPE). Methanol was evaporated under reduced pressure to yield fluorous allyl amine ("fluorous olefin") as an off-white solid. Two (2) equivalents of dithiothreitol (DTT, yielding "fluorous-DTT") or 1,4-butanedithiol (BDT, yielding "fluorous-BDT") and 2,2-dimethoxy-2-phenyl-acetophenone (DMPA, 10 mol % of dithiol) were added to a solution of corresponding fluorous-olefin in methanol (>80 mM). The reaction mixture was UV-irradiated for 270 s at 20 mW/cm^2. The product (fluorous-thiol) was purified by FSPE. The fluorous organic mixture was precipitated by adding one-fourth of the reaction volume of water and loaded onto the fluorous silica column. Any remaining fluorous material in the reaction vessel was resolubilized in methanol, again precipitated by water addition, and transferred to the fluorous column. A fluorophobic wash (20 vol% Water in MeOH) was used to elute all non-fluorous molecules while the fluorous-tagged material was retained on the fluorous silica gel (Thiolene wash: 0.33mL/mg of fluorous material; Michael addition wash: 0.5mL/mg of fluorous material). A fluorophilic wash of methanol was then used to elute the fluorous material (0.2mL/mg fluorous material). Methanol was removed by vacuum centrifuge or argon at 40C. The product was confirmed by NMR. Fluorous-DTT, off-white solid, ^{1}H NMR (400 MHz, Chloroform-d) δ 5.82 (m, 1H), 5.16 (m, 2H), 4.64 (m, 1H), 3.72 (m, 2H), 2.04 (m, 4H), 1.49 (s, 7H).

Quantification of the thiol-Michael addition kinetics. Monitoring the thiol-Michael addition is typically observed by FTIR, but was not possible in this case due to crowding in the spectra. Another general method for quantifying chemical reaction kinetics is through the use of high-performance liquid chromatography mass spectrometry (LCMS). However, kinetic quantification by dithiodipyridine (DTDP) was greatly favored over LCMS. Since the DTDP assay was performed in a 96-well assay, triplicate experiments could be completed in parallel to better determine experimental error. Additionally, data acquisition was immediate, utilizing a plate reader. The LCMS-based quantification would require significantly more time for data acquisition, even with shortened, direct injection runs. When preliminary experiments were complete, multiple washes between each run were required to re-establish a clean baseline and eliminate any persistent detection of the product mass. Moreover, some products from the monomers examined in this work demonstrated poor ionization or additional persistent detection in subsequent blank runs, convoluting quantitation. Therefore, the DTDP assay was utilized in a quantitative, high-throughput manner for kinetic analysis of our thiol-Michael additions. All data were plotted and analyzed in GraphPad Prism 7.05 using nonlinear regression fitting to an integrated solution of the bimolecular kinetic rate equation (see Supplementary Information).

The dithiodipyridine (DTDP) assay. The DTDP assay[69,70] was adapted to a 96-well plate format to measure the combined thiol and thiolate concentration and track the reaction conversion. Adaptions are detailed within the Supplemental Information (Figure S1). The thiol-Michael addition was performed across a variety of monomers at 30 mM fluorous (4-10mg, 6.8-17 μmol). 2 equivalents of

N-allyl-*N*-acrylamide monomer (13.6-34 μmol) from a 200mM methanol stock was activated for 15 minutes with 0.1 equivalents (5 mol% relative to *N*-allyl-*N*-acrylamide monomer) of dimethylphenyl phosphine (0.68-1.7 μmol DMPP) from a 2.5 v/v% stock in methanol. Reactions were performed at both room temperature (25°C) and elevated temperature (40°C). The kinetic rates of the reaction were analyzed by fitting a simple bimolecular rate equation to the data because all reactions contained the same DMPP equivalency as has been used in literature[9] (Figure 2A, see Supplemental Information).

Preceding each reaction, dimethylphenylphosphine (DMPP) was incubated with each *N*-allyl-*N*-acrylamide monomer for fifteen minutes to create the phosphine initiator, which acts as carbanion base (Figure 1 in blue). Fifteen (15) minutes was chosen as a phosphine incubation time from literature precedent demonstrating monomer incubation delayed reaction initiation, otherwise a delay would be observed while the carbanion is generated.[42] NMR experiments were also performed to verify the completion of the reaction between the phosphine nucleophile and all *N*-allyl-*N*-acrylamides during the incubation time allowed at 120mM in methanol (see Figure S9-S11 and Table S3). Then, to start the reaction, the fluorous thiol was added. These reactions were specifically designed to start the reaction at a constant concentration of carbanion to allow us to examine the balance between the rates of propagation, chain transfer, or any other rate-limitations. The products of the reactions with MeMon were confirmed by ^{1}H NMR after FSPE. From the reaction of F-DTT with the methyl N-allyl-N-acrylamide ("F-DTT-MeMon"). Off-white solid. ^{1}H NMR (600 MHz, Chloroform-*d*) δ 5.74 (m, 1H), 5.18 (m, 2H), 4.88 (m, 1H), 3.95 (m, 2H), 3.73 (m, 2H), 3.22 (m, 2H), 2.94 (d, J = 3.6 Hz, 3H), 2.92 – 2.56 (m, 11H), 2.06 (m, 4H), 1.78 (m, 2H), 1.46 (s, 6H). From the reaction of F-DTT with the methyl N-allyl-N-acrylamide ("F-BDT-MeMon"). Off-white solid. ^{1}H NMR (600 MHz, Chloroform-*d*) δ 5.75 (m, 1H), 5.18 (m, 2H), 4.77 (m, 1H), 3.95 (m, 2H), 3.22 (m, 2H), 2.93 (d, J = 7.1 Hz, 3H), 2.82 (q, J = 7.4 Hz 2H), 2.56 (m, 8H), 2.07 (m, 4H), 1.77 (m, 2H), 1.68 (m, 4H), 1.47 (s, 6H).

Computational. We determined the reaction energy corresponding to each of our experimentally studied Michael addition reactions using density functional theory (DFT) coupled with the Nudged Elastic Band (NEB) method,[71–73] we performed a step-by-step analysis to uncover the mechanism of reaction, along with the corresponding energy barriers. All simulations were run through Squid, the Clancy group codebase.[74] After isolating each step in the mechanism, the atomic geometry of all reactants, products, and intermediates were optimized by minimizing the electronic and nuclear energy in the system. The fluorous tail on the thiol was truncated at the amide group to improve computational speed, validated since the fluorous tail was far from the reactive site throughout the reaction mechanism. In some cases, the Cartesian coordinates of the end of the thiol tail were constrained to prohibit unphysical interactions between the truncated tail and the reactive complex. Once all minima were properly converged to their ground-state energies, the transition states were determined using the NEB method,[71–73] excluding product decomplexation which was approximated as the energy difference between a complexed and fully decomplexed product. The NEB method takes a series of intermediate atomic positions along a reaction coordinate as input, applies a fictitious spring force between these atomic positions, and minimizes the forces on each atomic position until the root mean square force converges to the minimum energy pathway. The spring force constrains each atomic position along the energy barrier from falling to an energy minimum while the potential energy gradient is minimized. Our initial atomic positions were approximated using a linear interpolation method that uses partial Procrustes superimposition to minimize translation and rigid rotation between positions.[75]

Once converged, the highest energy atomic position along the reaction coordinate was taken as the approximate transition state structure. To ensure that the converged transition state is physically correct, we vetted it using three criteria. First, the reactive atom for this transition state must lie at an intermediate distance between two chemical bonds. Second, the intrinsic reaction coordinate (IRC) must pass from the reactant to the product through our predicted transition state. Third, the transition state had to have one imaginary vibrational mode, corresponding to a first-order saddle point along the IRC. Imaginary modes below 70 cm^{-1} were considered to be numerical noise due to issues pertaining to the cavity construction in the CPCM implicit solvent model.[76] This was verified through IRC calculations. Due to the computational expense of these calculations, non-reactive species were excluded to speed up the calculation. For all reported transition states, these criteria were met.

Finally, to quantify the effect of explicit solvent molecules, four methanol molecules were introduced to each stationary point for each mechanism, equivalent to the four hydroxyl groups in the thiolate molecules. Previously converged stationary points were constrained, and the methanol molecules were allowed to optimize to their ground-state energy. Once the methanol molecules at each calculated stationary point converged, the final activation energies and heats of reaction were calculated. The effect of the explicit solvents on the butyl *N*-allyl-*N*-acrylamide mechanism is shown in Figure S22 and Tables S6-7 of the ESI.

All DFT calculations were performed using the Orca software package.[76] DFT requires an electron density functional, providing an approximation necessary to calculate the energy of a set of atoms, and a basis set, which represents electron orbitals using superimposed Gaussian functions. Preliminary geometry optimizations and NEB calculations were performed using the B97-D3 functional,[77] which involves the Generalized Gradient Approximation (GGA) tier on Jacob's Ladder,[78] and Ahlrichs' def2-TZVP basis set.[79–81] Both were recommended by Grimme *et al.* for their fast and accurate calculations.[82,83] We used our custom Climbing Image NEB algorithm, developed by Herbol *et al.* to operate in Orca.[84] All simulations were subjected to an implicit methanol solvent using the Conductor-Polarizable Continuum Model (CPCM).[85] Our choice of functional, basis set, and solvation model was benchmarked against the ωB97X-D3 functional, known to perform well in thiol-Michael addition systems. Energies were measured relative to the ground-state energy of the reactants of the initiation step for each mechanism. RLSs were identified as the step with the largest activation energy.

ASSOCIATED CONTENT

Electronic supplementary information is available. Protocols and data for chemical synthesis and identification, kinetic quantification, and analysis are provided along with details on computational approaches and calculations. Tabulated data for all experimental and computational

results are provided with statistical analysis where appropriate. Discussion concerning additional mechanistic pathways including calculations and experimental data are provided. Raw kinetic data with fits are included. Cartesian coordinates and energies of the DFT calculated stationary points are provided in a separate file titled "coordinates.xyz."

AUTHOR INFORMATION

Corresponding Author

* Correspondence should be addressed to: caa238@cornell.edu (experimental), pclancy3@jhu.edu (computational)

Present Addresses

†Present address: Department of Chemistry, Massachusetts Institute of Technology, Cambridge, MA, USA

Author Contributions

The manuscript was written through contributions of all authors, whom have provided final approval. ‡These authors contributed equally.

Funding Sources

Cornell University Start-Up funds (C.A.A.), National Science Foundation CAREER Award (CHE-1554046) (C.A.A.), Army Research Office (W911NF-15-10179) (C.A.A.), Nancy and Peter Meinig Investigator Fellowship (C.A.A.). Cornell Institute for Computational Science and Engineering (ICSE) (P.C.), Maryland Advanced Research Computing Center (MARCC) (P.C.), John Hopkins University Start-Up Funds (P.C.), NSERC Postgraduate Scholarships-Doctoral (PGS-D) award (CGSD3-502578-2017) (A.W.R.), National Science Foundation Graduate Research Fellowship Program (DBE-1144153) (J.S.B.)

ACKNOWLEDGMENT

This project was supported in part by Cornell University Start-Up funds (C.A.A.), the National Science Foundation CAREER Award (CHE-1554046), the Army Research Office (W911NF-15-10179), and the Nancy and Peter Meinig Investigator Fellowship (C.A.A.). The authors thank the Cornell Institute for Computational Science and Engineering (ICSE) and the Maryland Advanced Research Computing Center (MARCC) (P.C.) which is partially funded by the State of Maryland, for provision of computational resources. P.C. acknowledges Johns Hopkins University for financial support via start-up funding. A.W.R. gratefully acknowledges the financial support of the NSERC Postgraduate Scholarships-Doctoral (PGS-D) award (CGSD3-502578-2017) and the Cornell University Graduate School. J.S.B. acknowledges financial support from the National Science Foundation Graduate Research Fellowship Program (DBE-1144153). This work made use of the Cornell University NMR Facility, which is supported, in part, by NSF-MRI (CHE-1531632).

ABBREVIATIONS

oligoTEAs, oligothioetheramides; RLS, rate-limiting step; EWG, electron-withdrawing group; Nuc, nucleophile; DMPP, dimethylphenylphosphine; F-DTT, fluorous thiol; DFT, density functional theory; PES, Potential Energy Surface; NEB, Nudged Elastic Band; MEP, Minimum Energy Pathway; DTDP, dithiodipyridine; equivalent, eqv; fluorous solid-phase extraction, FSPE.

REFERENCES

(1) Hoyle, C. E.; Bowman, C. N. Thiol-Ene Click Chemistry. *Angew. Chemie - Int. Ed.* **2010**, *49* (9), 1540–1573. https://doi.org/10.1002/anie.200903924.

(2) Kade, M. J.; Burke, D. J.; Hawker, C. J. The Power of Thiol-Ene Chemistry. *J. Polym. Sci. Part A Polym. Chem.* **2010**, *48* (4), 743–750. https://doi.org/10.1002/pola.23824.

(3) Hoyle, C. E.; Lee, T. Y.; Roper, T. Thiol–Enes: Chemistry of the Past with Promise for the Future. *J. Polym. Sci. Part A Polym. Chem.* **2004**, *42* (21), 5301–5338. https://doi.org/10.1002/pola.20366.

(4) Lowe, A. B. Thiol-Ene "Click" Reactions and Recent Applications in Polymer and Materials Synthesis. *Polym. Chem.* **2010**, *1* (1), 17–36. https://doi.org/10.1039/B9PY00216B.

(5) Akiba, M. Vulcanization and Crosslinking in Elastomers. *Prog. Polym. Sci.* **1997**, *22* (3), 475–521. https://doi.org/10.1016/S0079-6700(96)00015-9.

(6) Li, G. Z.; Randev, R. K.; Soeriyadi, A. H.; Rees, G.; Boyer, C.; Tong, Z.; Davis, T. P.; Becer, C. R.; Haddleton, D. M. Investigation into Thiol-(Meth)Acrylate Michael Addition Reactions Using Amine and Phosphine Catalysts. *Polym. Chem.* **2010**, *1* (8), 1196–1204. https://doi.org/10.1039/c0py00100g.

(7) Michael, A. Ueber Die Addition von Natriumacetessig- Und Natriummalonsäureäthern Zu Den Aethern Ungesättigter Säuren. *J. für Prakt. Chemie* **1887**, *35* (1), 349–356. https://doi.org/10.1002/prac.18870350136.

(8) Tokoroyama, T. Discovery of the Michael Reaction. *European J. Org. Chem.* **2010**, *2010* (10), 2009–2016. https://doi.org/10.1002/ejoc.200901130.

(9) Nair, D. P.; Podgórski, M.; Chatani, S.; Gong, T.; Xi, W.; Fenoli, C. R.; Bowman, C. N. The Thiol-Michael Addition Click Reaction: A Powerful and Widely Used Tool in Materials Chemistry. *Chem. Mater.* **2014**, *26* (1), 724–744. https://doi.org/10.1021/cm402180t.

(10) Allen, C. F. H.; Fournier, J. O.; Humphlett, W. J. The Thermal Reversibility of the Michael Reaction:

IV. Thiol Adducts. *Can. J. Chem.* **1964**, *42* (11), 2616–2620. https://doi.org/10.1139/v64-383.

(11) Nising, C. F.; Bräse, S. The Oxa-Michael Reaction: From Recent Developments to Applications in Natural Product Synthesis. *Chem. Soc. Rev.* **2008**, *37* (6), 1218–1228. https://doi.org/10.1039/b718357g.

(12) Wang, X.; Li, S.; Jiang, Y. A Theoretical Study of the Mechanism of Phosphine-Catalyzed Hydroalkoxylation of Methyl Vinyl Ketone. *J. Phys. Chem. A* **2005**, *109* (47), 10770–10775. https://doi.org/10.1021/jp052426b.

(13) Desmet, G. B.; D'Hooge, D. R.; Omurtag, P. S.; Espeel, P.; Marin, G. B.; Du Prez, F. E.; Reyniers, M. F. Quantitative First-Principles Kinetic Modeling of the Aza-Michael Addition to Acrylates in Polar Aprotic Solvents. *J. Org. Chem.* **2016**, *81* (24), 12291–12302. https://doi.org/10.1021/acs.joc.6b02218.

(14) Hoyle, C. E.; Lowe, A. B.; Bowman, C. N. Thiol-Click Chemistry: A Multifaceted Toolbox for Small Molecule and Polymer Synthesis. *Chem. Soc. Rev.* **2010**, *39* (4), 1355. https://doi.org/10.1039/b901979k.

(15) Mather, B. D.; Viswanathan, K.; Miller, K. M.; Long, T. E. Michael Addition Reactions in Macromolecular Design for Emerging Technologies. *Prog. Polym. Sci.* **2006**, *31* (5), 487–531. https://doi.org/10.1016/j.progpolymsci.2006.03.001.

(16) Sun, Y.; Liu, H.; Cheng, L.; Zhu, S.; Cai, C.; Yang, T.; Yang, L.; Ding, P. Thiol Michael Addition Reaction: A Facile Tool for Introducing Peptides into Polymer-Based Gene Delivery Systems. *Polym. Int.* **2018**, *67* (1), 25–31. https://doi.org/10.1002/pi.5490.

(17) Frayne, S. H.; Northrop, B. H. Evaluating Nucleophile Byproduct Formation during Phosphine- and Amine-Promoted Thiol-Methyl Acrylate Reactions. *J. Org. Chem.* **2018**, *83* (17), 10370–10382. https://doi.org/10.1021/acs.joc.8b01471.

(18) Chen, J.; Jiang, X.; Carroll, S. L.; Huang, J.; Wang, J. Theoretical and Experimental Investigation of Thermodynamics and Kinetics of Thiol-Michael Addition Reactions: A Case Study of Reversible Fluorescent Probes for Glutathione Imaging in Single Cells. *Org. Lett.* **2015**, *17* (24), 5978–5981. https://doi.org/10.1021/acs.orglett.5b02910.

(19) Firouzabadi, H.; Iranpoor, N.; Jafari, A. A. Micellar Solution of Sodium Dodecyl Sulfate (SDS) Catalyzes Facile Michael Addition of Amines and Thiols to α,β-Unsaturated Ketones in Water under Neutral Conditions. *Adv. Synth. Catal.* **2005**, *347* (5), 655–661. https://doi.org/10.1002/adsc.200404348.

(20) Xi, W.; Pattanayak, S.; Wang, C.; Fairbanks, B.; Gong, T.; Wagner, J.; Kloxin, C. J.; Bowman, C. N. Clickable Nucleic Acids: Sequence-Controlled Periodic Copolymer/Oligomer Synthesis by Orthogonal Thiol-X Reactions. *Angew. Chem. Int. Ed. Engl.* **2015**, *54* (48), 14462–14467. https://doi.org/10.1002/anie.201506711.

(21) Xi, W.; Peng, H.; Aguirre-Soto, A.; Kloxin, C. J.; Stansbury, J. W.; Bowman, C. N. Spatial and Temporal Control of Thiol-Michael Addition via Photocaged Superbase in Photopatterning and Two-Stage Polymer Networks Formation. *Macromolecules* **2014**, *47* (18), 6159–6165. https://doi.org/10.1021/ma501366f.

(22) Seto, H.; Takara, M.; Yamashita, C.; Murakami, T.; Hasegawa, T.; Hoshino, Y.; Miura, Y. Surface Modification of Siliceous Materials Using Maleimidation and Various Functional Polymers Synthesized by Reversible Addition-Fragmentation Chain Transfer Polymerization. *ACS Appl. Mater. Interfaces* **2012**, *4* (10), 5125–5133. https://doi.org/10.1021/am301637q.

(23) Tedja, R.; Soeriyadi, A. H.; Whittaker, M. R.; Lim, M.; Marquis, C.; Boyer, C.; Davis, T. P.; Amal, R. Effect of TiO2 Nanoparticle Surface Functionalization on Protein Adsorption, Cellular Uptake and Cytotoxicity: The Attachment of PEG Comb Polymers Using Catalytic Chain Transfer and Thiol–Ene Chemistry. *Polym. Chem.* **2012**, *3* (10), 2743. https://doi.org/10.1039/c2py20450a.

(24) Liang, Y.; Li, L.; Scott, R. A.; Kiick, K. L. 50th Anniversary Perspective : Polymeric Biomaterials: Diverse Functions Enabled by Advances in Macromolecular Chemistry. *Macromolecules* **2017**, *50* (2), 483–502. https://doi.org/10.1021/acs.macromol.6b02389.

(25) Renault, K.; Fredy, J. W.; Renard, P. Y.; Sabot, C. Covalent Modification of Biomolecules through Maleimide-Based Labeling Strategies. *Bioconjug. Chem.* **2018**, *29* (8), 2497–2513. https://doi.org/10.1021/acs.bioconjchem.8b00252.

(26) Hong, V.; Kislukhin, A. A.; Finn, M. G. Thiol-Selective Fluorogenic Probes for Labeling and Release. *J. Am. Chem. Soc.* **2009**, *131* (29), 9986–9994. https://doi.org/10.1021/ja809345d.

(27) Northrop, B. H.; Frayne, S. H.; Choudhary, U. Thiol-Maleimide "Click" Chemistry: Evaluating the Influence of Solvent, Initiator, and Thiol on the Reaction Mechanism, Kinetics, and Selectivity. *Polym. Chem.* **2015**, *6* (18), 3415–3430. https://doi.org/10.1039/c5py00168d.

(28) Porel, M.; Alabi, C. A. Sequence-Defined Polymers via Orthogonal Allyl Acrylamide Building Blocks. *J. Am. Chem. Soc.* **2014**, *136* (38), 13162–13165. https://doi.org/10.1021/ja507262t.

(29) Porel, M.; Brown, J. S.; Alabi, C. A. Sequence-Defined Oligothioetheramides. *Synlett* **2015**, *26*, 565–571. https://doi.org/10.1055/s-0034-1380113.

(30) Sorkin, M. R.; Walker, J. A.; Brown, J. S.; Alabi, C. A. Versatile Platform for the Synthesis of Orthogonally Cleavable Heteromultifunctional Cross-Linkers. *Bioconjug. Chem.* **2017**, *28* (4), 907–912. https://doi.org/10.1021/acs.bioconjchem.7b00033.

(31) Brown, J. S.; Mohamed, Z. J.; Artim, C. M.; Thornlow, D. N.; Hassler, J. F.; Rigoglioso, V. P.; Daniel, S.; Alabi, C. A. Antibacterial Isoamphipathic Oligomers Highlight the Importance of Multimeric Lipid Aggregation for Antibacterial Potency. *Commun. Biol.* **2018**, *1* (1), 220. https://doi.org/10.1038/s42003-018-0230-4.

(32) Reizman, B. J.; Jensen, K. F. Feedback in Flow for Accelerated Reaction Development. *Acc. Chem. Res.* **2016**, *49* (9), 1786–1796. https://doi.org/10.1021/acs.accounts.6b00261.

(33) Mijalis, A. J.; Thomas, D. A.; Simon, M. D.; Adamo, A.; Beaumont, R.; Jensen, K. F.; Pentelute, B. L. A Fully Automated Flow-Based Approach for Accelerated Peptide Synthesis. *Nat. Chem. Biol.* **2017**, *13* (5), 464–466. https://doi.org/10.1038/nchembio.2318.

(34) Plutschack, M. B.; Pieber, B.; Gilmore, K.; Seeberger, P. H. The Hitchhiker's Guide to Flow Chemistry. *Chem. Rev.* **2017**, *117* (18), 11796–11893. https://doi.org/10.1021/acs.chemrev.7b00183.

(35) Murray, J. K.; Gellman, S. H. Parallel Synthesis of Peptide Libraries Using Microwave Irradiation. *Nat. Protoc.* **2007**, *2* (3), 624–631. https://doi.org/10.1038/nprot.2007.23.

(36) Wang, C.; Qi, C. Mechanistic Insights into N- or P-Centered Nucleophile Promoted Thiol–Vinylsulfone Michael Addition. *Tetrahedron* **2013**, *69* (26), 5348–5354. https://doi.org/10.1016/j.tet.2013.04.123.

(37) Chan, J. W.; Hoyle, C. E.; Lowe, A. B. Sequential Phosphine-Catalyzed, Nucleophilic Thiol–Ene/Radical-Mediated Thiol–Yne Reactions and the Facile Orthogonal Synthesis of Polyfunctional Materials. *J. Am. Chem. Soc.* **2009**, *131* (16), 5751–5753. https://doi.org/10.1021/ja8099135.

(38) Chan, J. W.; Hoyle, C. E.; Lowe, A. B.; Bowman, M. Nucleophile-Initiated Thiol-Michael Reactions: Effect of Organocatalyst, Thiol, and Ene. *Macromolecules* **2010**, *43* (15), 6381–6388. https://doi.org/10.1021/ma101069c.

(39) Jones, M. W.; Mantovani, G.; Ryan, S. M.; Wang, X.; Brayden, D. J.; Haddleton, D. M. Phosphine-Mediated One-Pot Thiol–Ene "Click" Approach to Polymer–Protein Conjugates. *Chem. Commun.* **2009**, No. 35, 5272. https://doi.org/10.1039/b906865a.

(40) Khire, V. S.; Lee, T. Y.; Bowman, C. N. Surface Modification Using Thiol–Acrylate Conjugate Addition Reactions. *Macromolecules* **2007**, *40* (16), 5669–5677. https://doi.org/10.1021/ma070146j.

(41) Xi, W.; Wang, C.; Kloxin, C. J.; Bowman, C. N. Nitrogen-Centered Nucleophile Catalyzed Thiol-Vinylsulfone Addition, Another Thiol-Ene "Click" Reaction. *ACS Macro Lett.* **2012**, *1* (Copyright (C) 2016 American Chemical Society (ACS). All Rights Reserved.), 811–814. https://doi.org/10.1021/mz3001918.

(42) Chatani, S.; Nair, D. P.; Bowman, C. N. Relative Reactivity and Selectivity of Vinyl Sulfones and Acrylates towards the Thiol–Michael Addition Reaction and Polymerization. *Polym. Chem.* **2013**, *4* (4), 1048–1055. https://doi.org/10.1039/C2PY20826A.

(43) Stewart, I. C.; Bergman, R. G.; Toste, F. D. Phosphine-Catalyzed Hydration and Hydroalkoxylation of Activated Olefins: Use of a Strong Nucleophile to Generate a Strong Base. *J. Am. Chem. Soc.* **2003**, *125* (29), 8696–8697. https://doi.org/10.1021/ja035232n.

(44) Desmet, G. B.; Sabbe, M. K.; D'Hooge, D. R.; Espeel, P.; Celasun, S.; Marin, G. B.; Du Prez, F. E.; Reyniers, M. F. Thiol-Michael Addition in Polar Aprotic Solvents: Nucleophilic Initiation or Base Catalysis? *Polym. Chem.* **2017**, *8* (8), 1341–1352. https://doi.org/10.1039/c7py00005g.

(45) Chan, J. W.; Hoyle, C. E.; Lowe, A. B.; Bowman, M. Nucleophile-Initiated Thiol-Michael Reactions: Effect of Organocatalyst, Thiol, and Ene. *Macromolecules* **2010**, *43* (15), 6381–6388. https://doi.org/10.1021/ma101069c.

(46) Zhang, D.-H.; Knelles, J.; Plietker, B. Iron-Catalyzed Michael Addition of Ketones to Polar Olefins. *Adv. Synth. Catal.* **2016**, *358* (15), 2469–2479. https://doi.org/10.1002/adsc.201600278.

(47) Krenske, E. H.; Petter, R. C.; Houk, K. N. Kinetics and Thermodynamics of Reversible Thiol Additions to Mono- and Diactivated Michael Acceptors: Implications for the Design of Drugs That Bind Covalently to Cysteines. *J. Org. Chem.* **2016**, *81* (23), 11726–11733. https://doi.org/10.1021/acs.joc.6b02188.

(48) Krenske, E. H.; Petter, R. C.; Zhu, Z.; Houk, K. N. Transition States and Energetics of Nucleophilic Additions of Thiols to Substituted α,β-Unsaturated Ketones: Substituent Effects Involve Enone Stabilization, Product Branching, and Solvation. *J. Org. Chem.* **2011**, *76* (12), 5074–5081. https://doi.org/10.1021/jo200761w.

(49) Galkin, V. I. Inductive Substituent Effects. *J. Phys. Org. Chem.* **1999**, *12* (4), 283–288. https://doi.org/10.1002/(SICI)1099-1395(199904)12:4<283::AID-POC126>3.0.CO;2-M.

(50) Sun, S.; Bernstein, E. R. Aromatic van Der Waals Clusters: Structure and Nonrigidity. *J. Phys. Chem.* **1996**, *100* (32), 13348–13366. https://doi.org/10.1021/jp960739o.

(51) Chelli, R.; Gervasio, F. L.; Procacci, P.; Schettino, V. Stacking and T-Shape Competition in Aromatic–Aromatic Amino Acid Interactions. *J. Am. Chem. Soc.* **2002**, *124* (21), 6133–6143. https://doi.org/10.1021/ja0121639.

(52) Huang, S.; Sinha, J.; Podgórski, M.; Zhang, X.; Claudino, M.; Bowman, C. N. Mechanistic Modeling of the Thiol–Michael Addition Polymerization Kinetics: Structural Effects of the Thiol and Vinyl Monomers. *Macromolecules* **2018**, *51* (15), 5979–5988. https://doi.org/10.1021/acs.macromol.8b01264.

(53) Li, G.-Z.; Randev, R.; Soeriyadi, A. H.; Rees, G. J.; Boyer, C.; Tong, Z.; Becer, C. R.; Haddleton, D. M. Investigation into Thiol-(Meth)Acrylate Michael Addition Reactions Using Amine and Phosphine Catalysts. *Polym. Chem.* **2010**, *1*, 1196–1204. https://doi.org/10.1039/c0py00100g.

(54) Smith, J. M.; Jami Alahmadi, Y.; Rowley, C. N. Range-Separated DFT Functionals Are Necessary to Model Thio-Michael Additions. *J. Chem. Theory Comput.* **2013**, *9* (11), 4860–4865. https://doi.org/10.1021/ct400773k.

(55) Awoonor-Williams, E.; Isley, W. C.; Dale, S. G.; Johnson, E. R.; Yu, H.; Becke, A. D.; Roux, B.; Rowley, C. N. Quantum Chemical Methods for Modeling Covalent Modification of Biological Thiols. *J. Comput. Chem.* **2020**, *41* (5), 427–438. https://doi.org/10.1002/jcc.26064.

(56) Mardirossian, N.; Head-Gordon, M. Thirty Years of Density Functional Theory in Computational Chemistry: An Overview and Extensive Assessment of 200 Density Functionals. *Mol. Phys.* **2017**, *115* (19), 2315–2372. https://doi.org/10.1080/00268976.2017.1333644.

(57) Swart, M.; van der Wijst, T.; Fonseca Guerra, C.; Bickelhaupt, F. M. Π-Π Stacking Tackled With Density Functional Theory. *J. Mol. Model.* **2007**, *13* (12), 1245–1257. https://doi.org/10.1007/s00894-007-0239-y.

(58) Plata, R. E.; Singleton, D. A. A Case Study of the Mechanism of Alcohol-Mediated Morita Baylis-Hillman Reactions. the Importance of Experimental Observations. *J. Am. Chem. Soc.* **2015**, *137* (11), 3811–3826. https://doi.org/10.1021/ja5111392.

(59) Exner, O. The Inductive Effect: Theory and Quantitative Assessment. *J. Phys. Org. Chem.* **1999**, *12* (4), 265–274. https://doi.org/10.1002/(SICI)1099-1395(199904)12:4<265::AID-POC124>3.0.CO;2-O.

(60) Charton, M. The Nature of Electrical Effect Transmission. *J. Phys. Org. Chem.* **1999**, *12* (4), 275–282. https://doi.org/10.1002/(SICI)1099-1395(199904)12:4<275::AID-POC125>3.0.CO;2-K.

(61) Tandon, R.; Nigst, T. A.; Zipse, H. Inductive Effects through Alkyl Groups - How Long Is Long Enough? *European J. Org. Chem.* **2013**, *2013* (24), 5423–5430. https://doi.org/10.1002/ejoc.201300486.

(62) Rai, N.; Siepmann, J. I. Transferable Potentials for Phase Equilibria. 9. Explicit Hydrogen Description of Benzene and Five-Membered and Six-Membered Heterocyclic Aromatic Compounds. *J. Phys. Chem. B* **2007**, *111* (36), 10790–10799. https://doi.org/10.1021/jp0735861.

(63) Cohen, A. J.; Mori-Sánchez, P.; Yang, W. Challenges for Density Functional Theory. *Chem. Rev.* **2012**, *112* (1), 289–320. https://doi.org/10.1021/cr200107z.

(64) Paul, R.; Paul, S. Synergistic Host–Guest Hydrophobic and Hydrogen Bonding Interactions in the Complexation between Endo-Functionalized Molecular Tube and Strongly Hydrophilic Guest Molecules in Aqueous Solution. *Phys. Chem. Chem. Phys.* **2018**, *20* (24), 16540–16550. https://doi.org/10.1039/C8CP01502C.

(65) Ryabenkova, Y.; Jadav, N.; Conte, M.; Hippler, M. F. A.; Reeves-McLaren, N.; Coates, P. D.; Twigg, P.; Paradkar, A. Mechanism of Hydrogen-Bonded Complex Formation between Ibuprofen and Nanocrystalline Hydroxyapatite. *Langmuir* **2017**, *33* (12), 2965–2976. https://doi.org/10.1021/acs.langmuir.6b04510.

(66) Bissantz, C.; Kuhn, B.; Stahl, M. A Medicinal Chemist's Guide to Molecular Interactions. *J. Med. Chem.* **2010**, *53* (14), 5061–5084. https://doi.org/10.1021/jm100112j.

(67) Sierański, T. Discovering the Stacking Landscape of a Pyridine-Pyridine System. *J. Mol. Model.* **2017**, *23* (12), 338. https://doi.org/10.1007/s00894-017-3496-4.

(68) Porel, M.; Thornlow, D. N.; Phan, N. N.; Alabi, C. A. Sequence-Defined Bioactive Macrocycles via an Acid-Catalysed Cascade Reaction. *Nat. Chem.* **2016**, *8* (6), 590–596. https://doi.org/10.1038/nchem.2508.

(69) Egwim, I. O.; Gruber, H. J. Spectrophotometric Measurement of Mercaptans with 4,4'-Dithiodipyridine. *Anal. Biochem.* **2001**, *288* (2), 188–194. https://doi.org/10.1006/abio.2000.4891.

(70) Grassetti, D. R.; Murray, J. F. Determination of Sulfhydryl Groups with 2,2'- or 4,4'-Dithiodipyridine. *Arch. Biochem. Biophys.* **1967**, *119* (1), 41–49. https://doi.org/10.1016/0003-9861(67)90426-2.

(71) Jónsson, H.; Mills, G.; Jacobsen, K. W. Nudged Elastic Band Method for Finding Minimum Energy Paths of Transitions. In *Classical and Quantum Dynamics in Condensed Phase Simulations*; World Scientific, 1998; pp 385–404. https://doi.org/10.1142/9789812839664_0016.

(72) Henkelman, G.; Uberuaga, B. P.; Jónsson, H. A Climbing Image Nudged Elastic Band Method for Finding Saddle Points and Minimum Energy Paths. *J. Chem. Phys.* **2000**, *113* (22), 9901–9904. https://doi.org/10.1063/1.1329672.

(73) Henkelman, G.; Jónsson, H. Improved Tangent Estimate in the Nudged Elastic Band Method for Finding Minimum Energy Paths and Saddle Points. *J. Chem. Phys.* **2000**, *113* (22), 9978–9985. https://doi.org/10.1063/1.1323224.

(74) Herbol, H. C.; Stevenson, J.; Acevedo, Y.; Ruttinger, A.; Clancy, P. Squid (Version Squid-v2.0.0a) https://zenodo.org/record/3360853#.XWljKShKhPY (accessed Aug 5, 2019). https://doi.org/10.5281/zenodo.3360853 Date Accessed: August 5th 2019.

(75) Eggert, D. W.; Lorusso, A.; Fisher, R. B. Estimating 3-D Rigid Body Transformations: A Comparison of Four Major Algorithms. *Mach. Vis. Appl.* **1997**, *9* (5–6), 272–290. https://doi.org/10.1007/s001380050048.

(76) Neese, F. The ORCA Program System. *Wiley Interdiscip. Rev. Comput. Mol. Sci.* **2012**, *2* (1), 73–78. https://doi.org/10.1002/wcms.81.

(77) Grimme, S. Semiempirical GGA-Type Density Functional Constructed with a Long-Range Dispersion Correction. *J. Comput. Chem.* **2006**, *27* (15), 1787–1799. https://doi.org/10.1002/jcc.20495.

(78) Perdew, J. P. Jacob's Ladder of Density Functional Approximations for the Exchange-Correlation Energy. In *AIP Conference Proceedings*; AIP, 2001; Vol. 577, pp 1–20. https://doi.org/10.1063/1.1390175.

(79) Schäfer, A.; Horn, H.; Ahlrichs, R. Fully Optimized Contracted Gaussian Basis Sets for Atoms Li to Kr. *J. Chem. Phys.* **1992**, *97* (4), 2571–2577. https://doi.org/10.1063/1.463096.

(80) Weigend, F.; Häser, M.; Patzelt, H.; Ahlrichs, R. RI-MP2: Optimized Auxiliary Basis Sets and Demonstration of Efficiency. *Chem. Phys. Lett.* **1998**, *294* (1–3), 143–152. https://doi.org/10.1016/S0009-2614(98)00862-8.

(81) Weigend, F.; Ahlrichs, R. Balanced Basis Sets of Split Valence, Triple Zeta Valence and Quadruple Zeta Valence Quality for H to Rn: Design and Assessment of Accuracy. *Phys. Chem. Chem. Phys.* **2005**, *7* (18), 3297. https://doi.org/10.1039/b508541a.

(82) Goerigk, L.; Grimme, S. A Thorough Benchmark of Density Functional Methods for General Main Group Thermochemistry, Kinetics, and Noncovalent Interactions. *Phys. Chem. Chem. Phys.* **2011**, *13* (14), 6670–6688. https://doi.org/10.1039/c0cp02984j.

(83) Goerigk, L.; Hansen, A.; Bauer, C.; Ehrlich, S.; Najibi, A.; Grimme, S. A Look at the Density Functional Theory Zoo with the Advanced GMTKN55 Database for General Main Group Thermochemistry, Kinetics and Noncovalent Interactions. *Phys. Chem. Chem. Phys.* **2017**, *19* (48), 32184–32215. https://doi.org/10.1039/c7cp04913g.

(84) Herbol, H. C.; Stevenson, J.; Clancy, P. Computational Implementation of Nudged Elastic Band, Rigid Rotation, and Corresponding Force Optimization. *J. Chem. Theory Comput.* **2017**, *13* (7), 3250–3259. https://doi.org/10.1021/acs.jctc.7b00360.

(85) Cossi, M.; Rega, N.; Scalmani, G.; Barone, V. Energies, Structures, and Electronic Properties of Molecules in Solution with the C-PCM Solvation Model. *J. Comput. Chem.* **2003**, *24* (6), 669–681. https://doi.org/10.1002/jcc.10189.

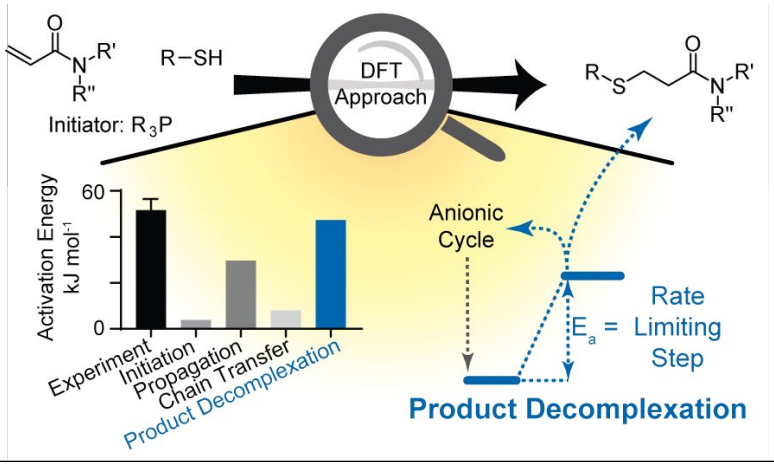
R–SH
DFT
Approach
Initiator: R3P
Activation Energy
kJ mol-1
60
0
Experiment
Initiation
Propagation
Chain Transfer
Product Decomplexation
Anionic
Cycle
Ea = Rate
Limiting
Step
Product Decomplexation

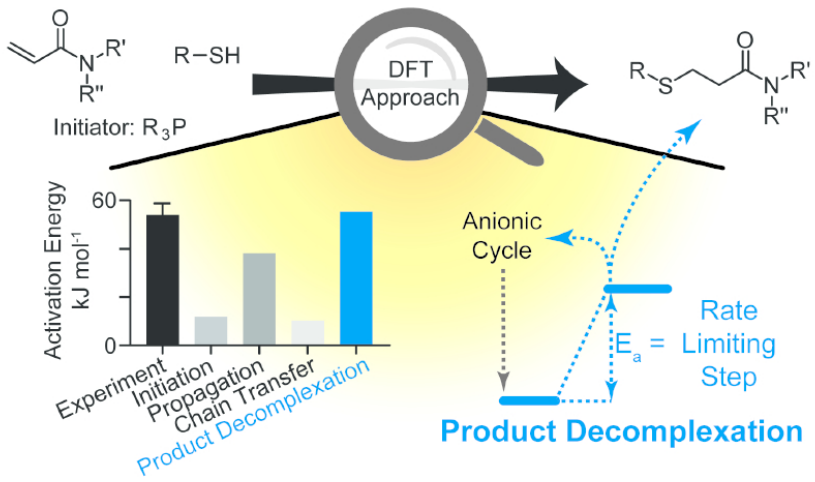

Experimental and computational agreement highlights rate-limiting "product decomplexation" and functional group effects in the thiol-Michael addition, utilized for sequence-defined oligomers.